*Australian Meteorological and Oceanographic Journal 63* (2013) 427–442

# Seasonal climate summary southern hemisphere (spring 2012): Warmer and drier across much of Australia, along with a new southern hemisphere sea ice extent record

**Phillip A. Reid[1], Matthew B. Tully[2], Andrew R. Klekociuk[3], Paul B. Krummel[4] and Stephen K. Rhodes[2]**

[1]Centre for Australian Weather and Climate Research (CAWCR), Bureau of Meteorology, Australia

[2]Bureau of Meteorology, Australia

[3]Australian Antarctic Division, Australia

[1]Centre for Australian Weather and Climate Research (CAWCR), CSIRO, Australia

(Manuscript received August 2013; revised January 2014)

Atmospheric, oceanic and sea ice conditions in the southern hemisphere are reviewed for the austral spring of 2012, with emphasis given to the Pacific basin climate indicators and Australian rainfall and temperature patterns. The Pacific basin saw a return to neutral ENSO conditions, with slightly warmer than normal equatorial SSTs just east of the date line and neutral SOI and multivariate ENSO indices. The Australian rainfall pattern was indicative of a positive Indian Ocean Dipole, with much of South Australia and other eastern Australian States experiencing much drier than normal conditions. Much of Western Australia, however, had a wetter than normal spring. November 2012 saw much of Australia's east and south experience one of the most significant spring heatwaves on record which, together with the dry conditions, would leave this area of the continent vulnerable to summer bushfires. Particularly strong cyclonic activity in the Ross Sea and off Queen Maud Land saw southern hemisphere sea ice reach a new record extent in September 2012 of approximately 19.45 million km$^2$.

## Introduction

This summary reviews the southern hemisphere and equatorial climate patterns for spring 2012, with particular attention given to the Australasian and Pacific regions, and a small section discussing Antarctic sea ice. The main sources of information for this report are analyses prepared by the Bureau of Meteorology's National Climate Centre and the Centre for Australian Weather and Climate Research (CAWCR).

*Corresponding author address:* Phillip Reid, CAWCR, Bureau of Meteorology, GPO Box 1289, Melbourne Vic. 3001, Australia.

## Indo-Pacific Basin climate

### Southern Oscillation Index

The Troup Southern Oscillation Index[1] (SOI) is based on the mean sea-level pressure (MSLP) difference between Tahiti and Darwin. Sustained values below –8 generally indicate an El Niño event, while sustained positive values above +8 are associated with La Niña periods. Figure 1 shows monthly SOI values from January 2009 through November 2012, together with a five-month weighted moving average.

The SOI shifted from weakly negative in autumn and winter 2012 (Martin 2013, Pepler 2013) to weakly positive in

[1]The Troup Southern Oscillation Index (Troup 1965) used in this article is ten times the standardised monthly anomaly of the difference in mean-sea-level pressure (MSLP) between Tahiti and Darwin. The calculation is based on a 60-year climatology (1933–1992). The Darwin MSLP is provided by the Bureau of Meteorology, and the Tahiti MSLP is provided by Météo France inter-regional direction for French Polynesia. All data are available at www.bom.gov.au/climate/current/soihtm1.shtml.

Fig. 1. Southern Oscillation Index, from January 2009 through November 2012, together with a five-month binomially weighted moving average. Means and standard deviations used in the computation of the SOI are based on the period 1933–1992.


Fig. 2. 5VAR composite standardised monthly ENSO index from January 2009 through November 2012, together with a weighted three-month moving average. See text for details.

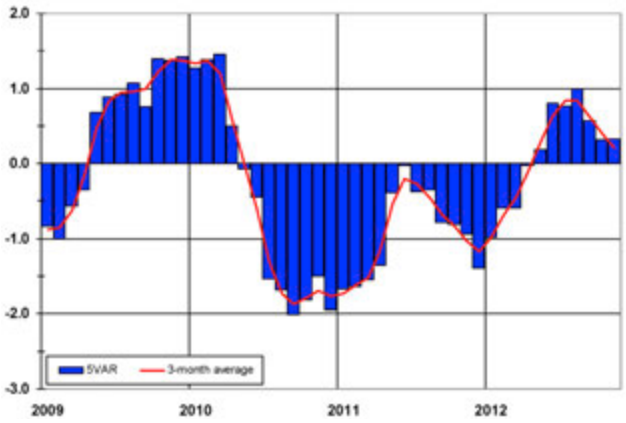


spring, continuing the neutral ENSO conditions established in autumn 2012. Monthly SOI values for spring 2012 were +2.7 (September), +2.4 (October) and +3.9 (November) for an average spring value of +3.0. Spring MSLP anomalies were positive at both Darwin and Tahiti, with Tahiti (+0.7 hPa) showing slightly stronger anomalies than Darwin (+0.3 hPa).

### Multivariate ENSO indices

Composite multivariate El Niño–Southern Oscillation (ENSO) indices are often regarded as more complete indicators of ENSO activity than those based solely on one variable, such as MSLP or sea surface temperature (SST), as they bring several atmospheric and oceanic parameters together.

The 5VAR[2] index is one such multivariate ENSO index (Kuleshov et al. 2009), calculated as the standardised amplitude of the first principal component of monthly Darwin and Tahiti MSLP[3] and monthly NINO3, NINO3.4 and NINO4 SST[4]. Following two years of negative 5VAR values associated with the 2010–11 and 2011–12 La Niña events (Fig. 2), 5VAR values rose through autumn (Martin 2013) and winter (Pepler 2013) 2012, peaking in August 2012 with a moderate value of +1.0. The 5VAR index then fell during spring 2012 to be close to neutral. Monthly 5VAR values for spring 2012 were +0.57 (September), +0.32 (October) and +0.33 (November) for an average spring value of +0.41.

Another index is the Multivariate ENSO Index[5] (MEI), produced by the US Climate Diagnostics Center, and is derived from a number of atmospheric and oceanic parameters calculated as a two-month mean. As with 5VAR, significant negative (positive) anomalies in the MEI are usually associated with La Niña (El Niño) events. Monthly MEI values for spring 2012 were +0.27 (August–September), +0.10 (September–October) and +0.17 (October–November) for an average spring value of +0.18, and are consistent with the sign of 5VAR and represent neutral ENSO conditions.

It is interesting to compare the respective signs of the multivariate ENSO indices against those of the SOI, from Fig. 1. SOI values are suggestive of slightly cool ENSO conditions, however when variables other than the strength of the atmospheric circulation are taken into account, as per the multivariate indices, ENSO conditions are slightly warm.

### Outgoing long-wave radiation

Deep convection in the equatorial Pacific can be measured, to a large degree, by the outgoing long-wave radiation (OLR), with decreases in OLR associated with increases in convection, and vice versa. Convection in the equatorial region, centred about the Date Line, is sensitive to changes in the Walker Circulation. Studies such as Hoerling et al. (1997) have shown that during El Niño events, OLR is generally reduced (that is, convection is enhanced) along the equator, particularly near and east of the Date Line. During La Niña events, OLR is often increased (that is, convection is suppressed) along the equator, particularly near and west of the Date Line. This was the case in spring 2011 (Fig. 3 in Cottrill 2012), where there was increased OLR along the equatorial region from 160°E through 180°E. Subsequent to this, La Niña conditions returned during 2011.

Standardised monthly anomalies[6] of OLR are computed by the Climate Prediction Center, Washington, over the equatorial Pacific region near the Date Line, ranging from

[2]ENSO 5VAR was developed at the Bureau's National Climate Centre and is described in Kuleshov et al. 2009. The principal component analysis and standardisation of this ENSO index is performed over the period 1950–1999.

[3]MSLP data obtained from www.bom.gov.au/climate/current/soihtm1.shtml. As previously mentioned, the Tahiti MSLP data are provided by Météo France inter-regional direction for French Polynesia.

[4]SST indices obtained from ftp://ftp.cpc.ncep.noaa.gov/wd52dg/data/indices/sstoi.indices.

[5]Multivariate ENSO Index obtained from www.esrl.noaa.gov/psd/people/klaus.wolter/MEI/table.html. The MEI is a standardised anomaly index described in Wolter and Timlin 1993 and 1998.

[6]Standardised monthly OLR anomalies are obtained from www.cpc.ncep.noaa.gov/data/indices/olr

Fig. 3. OLR anomalies for spring 2012 (W m$^{-2}$). Base period 1979–2000. The mapped region extends from 40°S to 40°N and from 70°E to 180°E.

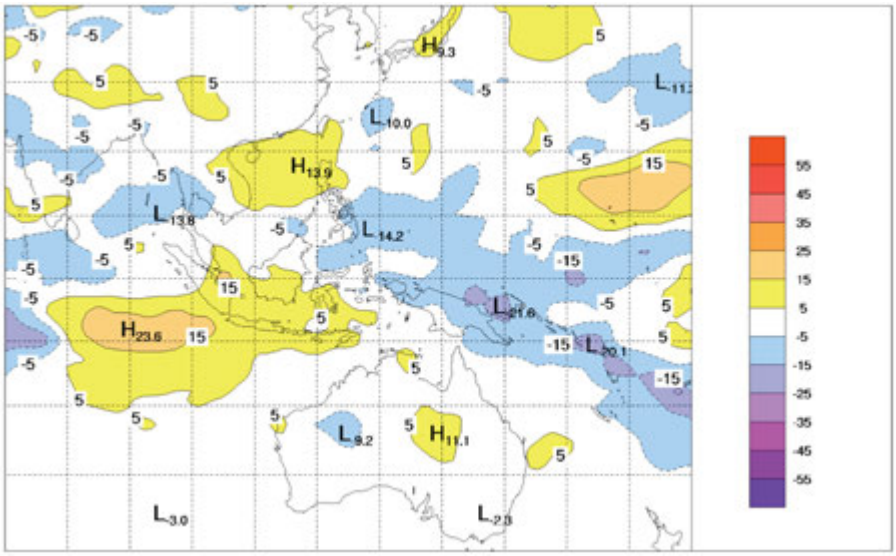


5°S to 5°N and 160°E to 160°W. From their analysis, monthly standardised OLR anomalies for spring 2012 were –0.4, –0.2 and 0.0 for September, October and November respectively, indicating overall marginally enhanced convection in this region and consistent with neutral ENSO conditions.

OLR values across the Indian and Pacific oceans for spring 2012 are displayed in Fig. 3. The Australian continent shows only minor departures from the long-term mean of OLR and only in relatively small areas; although these regions are generally consistent with associated rainfall deciles (see Fig. 20). Negative OLR anomalies dominate the equatorial western Pacific and are consistent with reports of heavy rainfall in this region: e.g. severe flooding in Papua New Guinea during early September. Positive OLR anomalies spread throughout much of the eastern Indian Ocean just south of the equator, and would represent suppressed convective activity in this region. This region of positive OLR anomalies encompasses the eastern 'pole' of the Indian Ocean Dipole (90°E to 110°E and 10°S to 0°S), as discussed below. Worth mentioning also is the band of anomalously low OLR stretching southeast from the equator at about 150°E (near Papua New Guinea). This would represent a well formed band of convective activity following along the South Pacific Convergence Zone (SPCZ), and is further discussed below in the section 'Sea surface temperatures'.

The static seasonal map of OLR (Fig. 3) hides considerable variability in the movement of convective activity, as simulated by OLR. The time-longitude plot of OLR anomalies (Fig. 4) shows the temporal evolution of these anomalies along the equatorial region (10ºS to 10ºN). From early September 2012 through early November 2012 the pattern of OLR anomalies is quite reasonably consistent with the pattern of spring 2011: negative OLR anomalies (implying enhanced convective activity) in the far western Pacific during late September/early October; negative OLR anomalies transitioning across the Indian Ocean during late October and early November; and positive OLR anomalies (implying reduced convective activity) transitioning across the Indian Ocean during late September/early October. However, the pattern of OLR activity differs from mid-November; in 2011 a second band of negative OLR anomalies transitioned across the equatorial Indian Ocean and through into the far western Pacific; in 2012 there is no secondary band of negative OLR. These differences may be crucial in the formation of ENSO events, where convective activity in the far western Pacific helps to strengthen the Walker Circulation which, given the right conditions in the equatorial Pacific, would enhance the prospect of a La Niña developing. This was the case in 2011.

## Madden-Julian Oscillation

The Madden-Julian Oscillation (MJO) is the major source of intraseasonal variability in the tropics. An active MJO is characterised by an eastward-propagating atmospheric anomaly near the equator that typically recurs every 30 to 60 days. It can often be detected by areas of strong negative equatorial OLR anomalies (a proxy for enhanced convective activity) that develop in the Indian Ocean and propagate eastward into the Pacific Ocean (Zhang 2005, Donald et al. 2006). The real-time Multivariate MJO (RMM) index developed by Wheeler and Hendon (2004) provides a method for monitoring the MJO, combining OLR data with 850 hPa and 200 hPa zonal winds to measure the state of the MJO each day. This index can be plotted in a phase-space diagram, as shown in Fig. 5 for spring 2012 and can be readily compared to the time-longitude plot of OLR anomalies shown in Fig. 4.

There was little in the way of persistent MJO activity during spring 2012, although the phase-space diagram does capture the passage of the small transient OLR anomalies

Fig. 4. Time-longitude section of daily-averaged OLR anomalies, averaged for 10°S to 10°N, for the period December 2010 through November 2012. Anomalies are with respect to a base period of 1979–2001.

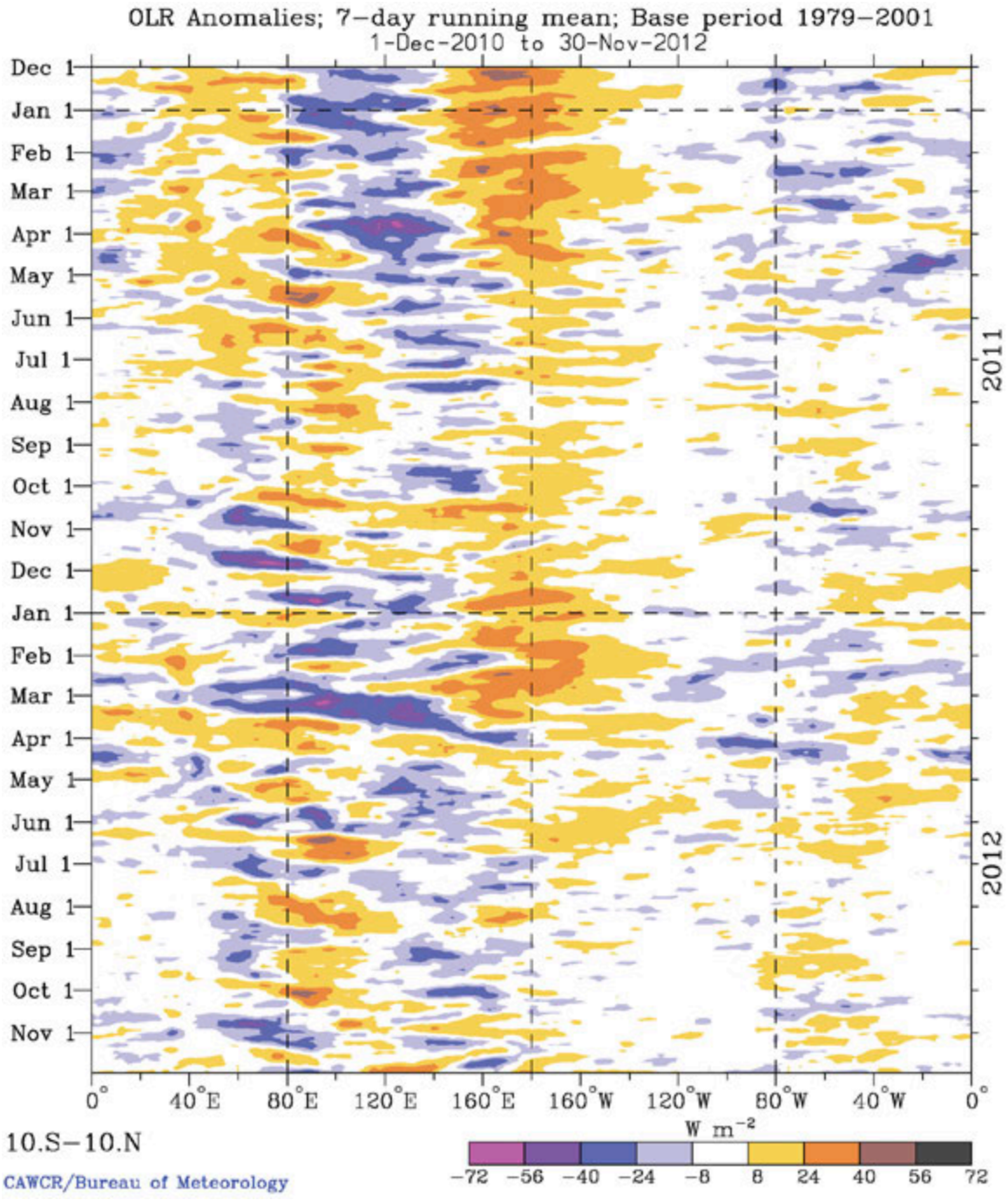


from Fig. 4. In particular, strong MJO activity is shown to occur from early through mid-September over the Maritime Continent and again from late September through early October towards the western Pacific. Further MJO activity occurs from mid to late October, passing through phase spaces one and two (across Africa and much of the Indian Ocean). In spring 2011 (Cottrill 2012, Fig. 5) we can see that the MJO is considerably more active and extensive compared to that of 2012, with the 2011 spring season finishing with strong activity through the central and eastern Indian Ocean. The apparent similarities in time-longitude OLR plots for springs in 2011 and 2012 compared to the marked differences in the strengths of the MJO activity and the subsequently different outcomes in ENSO events for these two years (La Niña in 2011 versus neutral in 2012) shows the importance of the holistic approach of the Multivariate MJO index in monitoring the Indo-Pacific climate basin.

As mentioned above, the impacts of the MJO, through

Fig. 5. Phase-space representation of the MJO index (Wheeler and Hendon 2004) for spring 2012. Daily values are shown with September in red, October in blue and November in yellow. The eight MJO phases and corresponding approximate locations of the near-equatorial enhanced convective signal are labelled. Strong MJO activity is associated with daily values outside the unit circle.

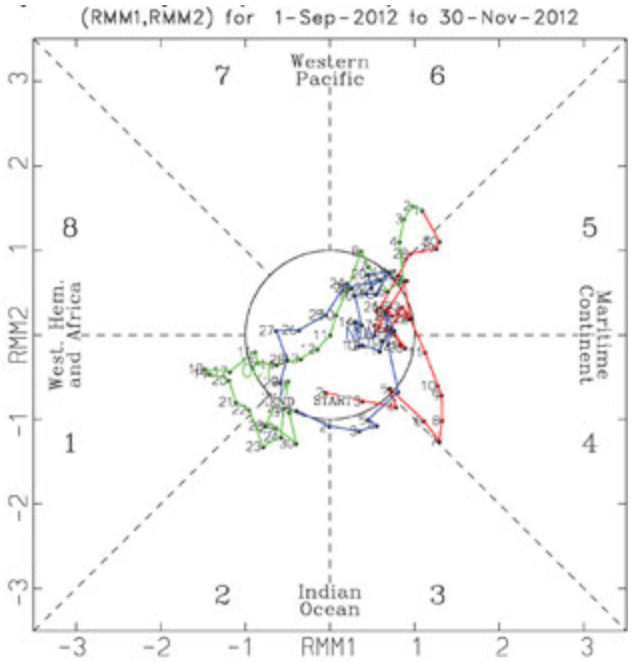


during early to mid-September, consistent with the heavy rainfall and flooding events that occurred in Papua New Guinea during that time.

### Indian Ocean Dipole

The Indian Ocean Dipole (IOD) is a coupled ocean and atmosphere phenomenon in the equatorial Indian Ocean that impacts on the climate of Australia and other countries surrounding the Indian Ocean basin (Saji et al. 1999). A positive IOD period has been shown[7] to be associated with a decrease in winter–spring rainfall over parts of central and southern Australia, while a negative IOD is generally associated with an increase in winter–spring rainfall over southern Australia.

The IOD is commonly measured by the Dipole Mode Index (DMI) that is the difference between sea surface temperature (SST) anomalies in the western (50°E to 70°E and 10°S to 10°N) and eastern (90°E to 110°E and 10°S to 0°S) equatorial Indian Ocean. Positive DMI, and hence positive IOD, implies colder SSTs in the eastern sector, while negative DMI implies warmer SSTs in the eastern sector. Weekly DMI values[8] (Fig. 6) were positive through most of spring 2012, peaking in early September, indicating a positive IOD event through the season. Australian rainfall was consistent with

[7]See for example www.bom.gov.au/climate/IOD/about_IOD.shtml and Risbey et al. 2009.
[8]Available at www.bom.gov.au/climate/enso/iod_1.txt

Fig. 6. Weekly Dipole Mode Index (DMI), a measure of the Indian Ocean Dipole, from weeks ending 4 January 2009 through 2 December 2012, together with a five-week weighted moving average. See text for details.

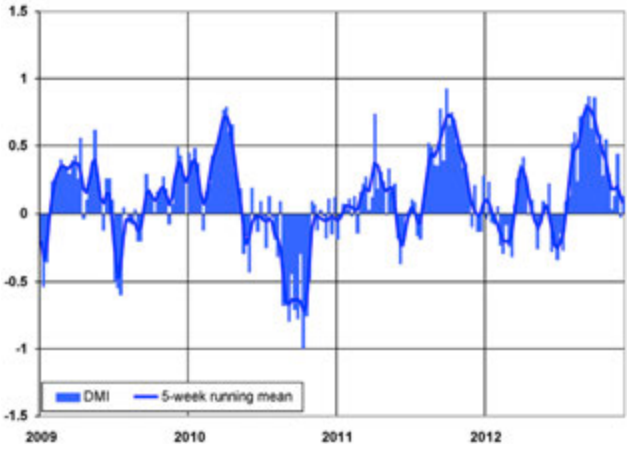


the positive period of the IOD, as shown below.

An interesting comparison can be made between DMI values from 2011 and that of 2012 and the Australian rainfall during these seasons. In general DMI values from spring 2011 and 2012 are quite similar in their timing and magnitude although in 2011 Australian rainfall was influenced by a positive IOD and a La Niña, while in 2012 Australian rainfall was influenced by a positive IOD and neutral ENSO conditions. The differences in rainfall will be highlighted below.

## Oceanic patterns

### Sea-surface temperatures

Global SST anomalies for spring 2012 are shown in Fig. 7. These are based on the US National Oceanic and Atmospheric Administration (NOAA) Optimum Interpolation analyses (Reynolds et al. 2002) dataset, with the climatological base period of 1971–2000. Warming in the equatorial Pacific basin is confined to a relatively small warm pool predominantly centred just to the west of the Date Line. Running to the southeast of this pool are asymmetric warm anomalies following generally along the line of the South Pacific Convergence Zone (SPCZ). The SPCZ SST anomalies are consistent with the negative OLR anomalies (enhanced convective activity) spreading southeast from the equator at around 160°E (Fig. 3). SSTs in the tropical Indian Ocean were warmer than average centred predominantly at around 60°E, coinciding with the western sector of the IOD, contributing to the positive DMI (Fig. 6). Around Australia, SSTs were warm to the west but overall average elsewhere; although during September (November) they were up to 2 °C cooler (warmer) along northern West Australian and Northern Territory coasts (not shown).

Compared to the previous season, winter 2012 (Fig. 5, Pepler 2013), the warm pool in the Pacific Basin transitioned

Fig. 7. Sea surface temperature anomalies for spring 2012 (°C).

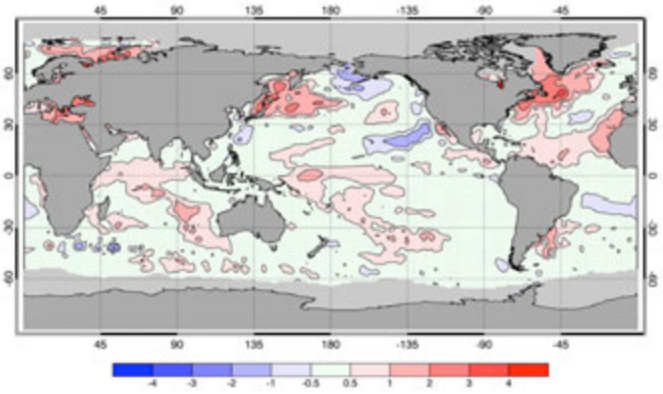

from the eastern to the western Pacific. SSTs in the eastern Pacific gradually cooled while in the western Pacific they gradually warmed. This is reflected in standard monthly NINO indices[9] where NINO1+2 lowered from 0.49 °C in September to –0.38 °C in November. Conversely, NINO4 increased marginally from 0.43 °C in September to 0.54 °C in November.

It is worth mentioning here the importance of the SPCZ on the development or decay of ENSO events. In mid-2012, based on the Composite ENSO Index (Fig. 2), SOI (Fig. 1) and analysis of climate models in mid-June 2012[10] there was the potential for the development of the El Niño during spring 2012. However, McGregor et al. (2012) concludes that the development of a SPCZ has a considerable contribution to the termination of El Niño events. In this particular case it may be that the formation of the SPCZ in spring helped terminate the development of an El Niño event.

### Subsurface patterns

The ocean thermocline is a distinct layer within which the temperature changes more rapidly with depth than it does in the layers above or below it. The thermocline can also be regarded as the boundary between the well-mixed upper ocean warm water and the cold deep water below. The position (depth) of the thermocline can be represented along the equator by the depth of the 20 °C isotherm. Due to the Walker Circulation's impact on the ocean surface, on average the thermocline has a depth of about 150 metres in the western Pacific, rising to about 50 metres in the eastern Pacific. ENSO events change the depth of the thermocline: La Niña magnifies the tilt while El Niño reduces the tilt.

Figure 8 shows time-longitude diagrams of (a) zonal wind anomalies averaged along 2°S to 2°N where positive is a westerly wind burst (or strengthening of the Walker Circulation); (b) 20 °C isotherm depth anomaly along 2°S to 2°N where positive (negative) represents a deeper (shallower) thermocline; and (c) 20 °C isotherm depth anomaly along 5°N. Quite obvious from Fig. 8(a) are the (negative) winds associated with the strengthening of the Walker Circulation from May through December 2010 and September 2011 through March 2012. These lead to the respective equatorial isotherm depth anomalies (Fig. 8(b)) associated with the La Niña events over those periods (Bureau of Meteorology 2012a, Ganter 2010, Lovitt 2011, Cottrill 2012 and Webb 2012). Also evident are the downwelling equatorial Kelvin waves (positive isotherm depth anomalies in Fig. 8(b)) that traverse the Pacific from west to east during the summer of 2010–11 and summer through autumn of 2011–2012: both of which lead to the slow moving off-equatorial downwelling Rossby waves (positive isotherm depth anomalies) traversing from east to west in Fig. 8(c).

Equatorial upper Pacific Ocean conditions for spring 2012 were the result of a combination of ocean and atmospheric interactions that occurred over the preceding 12 months or more. The slow moving off-equatorial upwelling Rossby wave that moved from east to west during 2012 (negative isotherm depth anomaly in Fig. 8(c)) provided the cold pool of water in the western Pacific. While the eastern Pacific warm pool is the result of the downwelling equatorial Kelvin wave traversing from west to east at the same time (positive isotherm depth anomalies in Fig. 8(b)). These provide the necessary ocean conditions for the potential formation of an El Niño. Sustained and strong westerly wind bursts are required to maintain these conditions and develop a mature El Niño. Small westerly wind bursts did occur from about May 2012 (Fig. 8(a)), although these were neither strong enough nor far enough east to continue the development of an El Niño.

Figure 9 shows a cross-section of equatorial subsurface temperature anomalies by month between August and November 2012. Compared to the same time the previous year (Fig. 9, Cottrill 2012) these anomalies are smaller in magnitude and extent and support the neutral ENSO conditions as described above. During this sequence a small cold pool develops at around 90°W and is indicative of increased upwelling in that region associated with a locally enhanced Walker Circulation (slightly stronger easterlies) off the coast of South America (Fig. 8(a)). El Niño conditions are very unlikely to develop in this scenario. Further to the west are small warm pools which contract to west of the date line as the season progresses.

### Sea ice

Here we use two general terms for measurement of southern hemisphere sea ice: concentration (per cent), the percentage of an area (here a 25 km × 25 km pixel) covered in sea ice; and sea ice extent (km$^2$), the area of sea ice with a concentration of 15 per cent or more. During September 2012 southern hemisphere sea ice achieved new sea ice extent daily (approximately 19.45 million km$^2$ on 22 September) and monthly average (19.36 million km$^2$) records since satellite

[9]NINO indices are SST anomalies (1971–2000 base period) averaged over NINO regions, described here www.bom.gov.au/climate/ahead/about-ENSO-outlooks.shtml and available from ftp://ftp.cpc.ncep.noaa.gov/wd52dg/data/indices/sstoi.indices

[10]See the Bureau of Meteorology's ENSO Wrap-up at www.bom.gov.au/climate/enso/archive/ensowrap_20120619.pdf

Fig. 8. Time-longitude section of the monthly anomalous (a) zonal surface winds and (b) depth of the 20 °C isotherm at the equator (2°S to 2°N), and (c) depth of the 20 °C isotherm at 5°N for January 2010 through November 2012. (Plot obtained from the TAO Project Office).

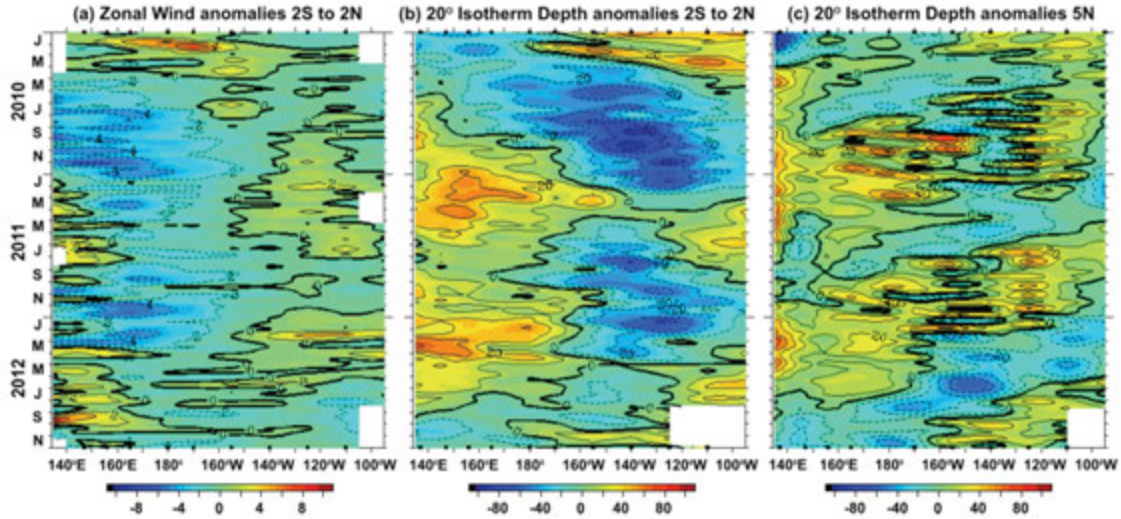


Fig. 9. Four-month August 2012 through November 2012 sequence of vertical sea subsurface temperature anomalies at the equator for the Pacific Ocean. The contour interval is 0.5 °C. (Plot obtained from CAWCR).

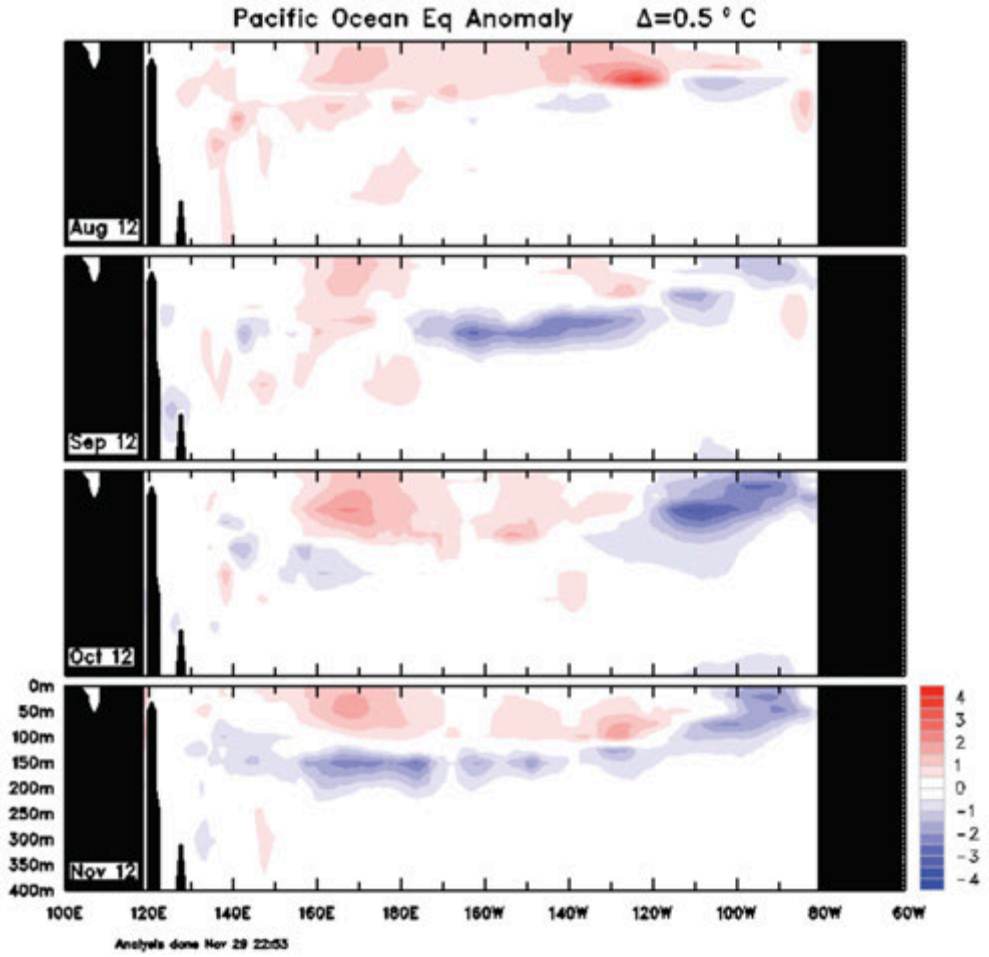

Fig. 10. Southern hemisphere sea ice concentration anomaly (per cent) with mean MSLP contours (ACCESS) for September 2012. Anomalies are calculated with respect to the 1981–2010 climatology.

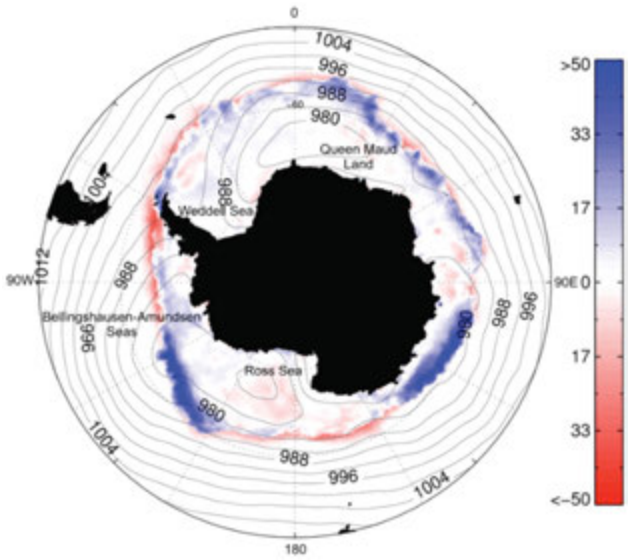


Fig. 11. Southern hemisphere sea ice extent anomaly (km$^2$ × 10$^6$) for each September from 1979 through 2012, along with the five-year weighted average. Anomalies are calculated with respect to the 1981–2010 climatology.

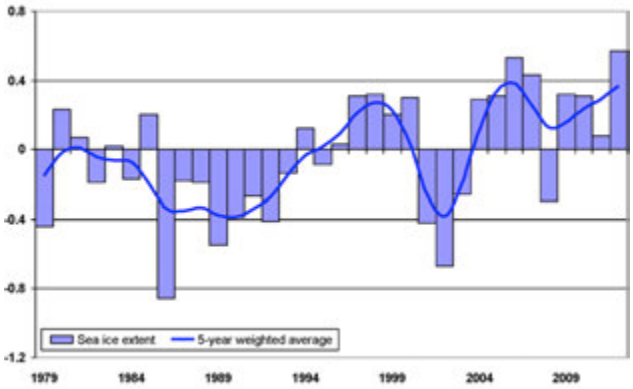


records began in 1978. Figure 10 shows the map of sea ice concentration anomalies for September 2012, along with monthly mean MSLP contours. The anomalous pattern in sea ice concentration is the result of earlier dynamic processes, with particularly strong and persistent cyclonic activity in the Bellingshausen-Amundsen Seas and Queen Maud Land regions during July and August which was responsible for an increase in sea ice extent in the eastern Ross Sea/Queen Maud Land. Above-average sea ice extents along parts of the East Antarctic coast (110°E–130°E) were synonymous with strong compaction and thickening of the ice by northerly winds in this region. Conversely, relatively warm northerly winds in July and August were responsible for inhibiting sea ice advance and subsequent lower than normal sea ice extents in the far eastern East Antarctic (150°E–180°E) and the western Weddell Sea. The pattern of sea ice concentration anomalies for September 2012 are consistent with the findings of Stammerjohn et al. (2008) in which we have positive Southern Annular Mode (SAM—see below) conditions during the mid-advance season causing a deepening of the Amundsen Sea Low, although in this particular season the low is centred further west towards the Ross Sea. In October 2012 southern hemisphere sea ice began to retreat and by the end of November was just below the long term average for that month.

Figure 11 shows the net monthly mean southern hemisphere sea ice extent anomalies for each September from 1979 through 2012. There is considerable interannual variability; there is also a positive trend of about 0.9 (+/-0.6) per cent per decade. This plot (Fig. 11) hides variability in the spatial pattern of changes. These local changes are a result of dynamic (synoptic) and thermodynamic changes, depending upon the region (Holland and Kwok 2012). Statistically significant changes also exist in the seasonality of southern hemisphere sea ice (Stammerjohn et al. 2012, Massom et al. 2013).

## Atmospheric patterns

### Surface analyses

The southern hemisphere spring 2012 MSLP pattern is shown in Fig. 12 and the associated anomaly pattern is shown in Fig. 13, the latter being calculated from the 1979–2000 climatology obtained from the National Centers for Environmental Prediction (NCEP) II Reanalysis data (Kanamitsu et al. 2002). Grey shading in Fig. 13 represents elevated areas, for which MSLP anomalies have not been calculated. The subtropical ridge is close to its climatological position with minor departures over the Australian continent and western Africa. The circumpolar trough is well defined and in close climatological position, although major departures in depth exist with a deepening north of the Ross Sea, at around 170°W, and positive anomaly further to the east and south in the Bellingshausen/Amundsen Seas. The lack of asymmetry or strong three-wave pattern is a result of a transition from positive to negative SAM (see below) during this season.

### Mid-tropospheric analyses

The southern hemisphere spring 2012 500 hPa geopotential height, which gives an indication of the steering of surface synoptic systems, is shown in Fig. 14 with the associated anomalies in Fig. 15. The geopotential flow in the mid-latitudes is quite zonal, although at higher southern latitudes a weak three-wave pattern becomes evident. Due to the orientation and relative positions of the positive anomaly over southern Australia and a negative anomaly to the southeast of New Zealand synoptic systems over southeast Australia would have had a northeasterly direction and would generally have been steered away from the continent

Fig. 12. Spring 2012 MSLP (hPa). The contour interval is 5 hPa.

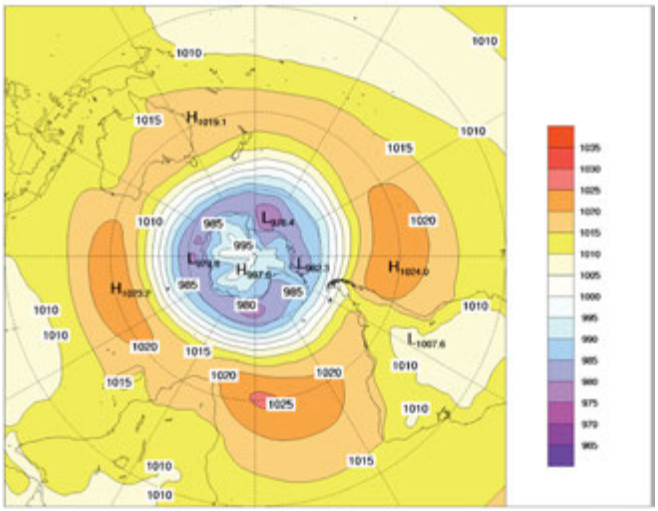

Fig. 13. Southern hemisphere spring 2012 MSLP anomalies (hPa), from a 1979–2000 climatology.

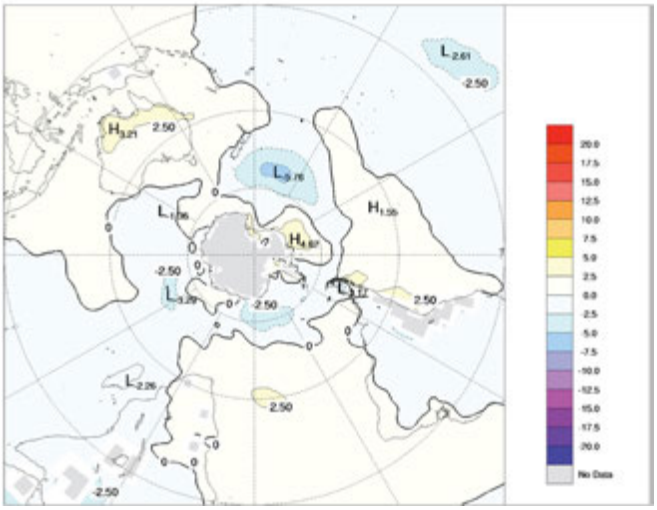

Fig. 14. Spring 2012 500 hPa mean geopotential height (gpm).

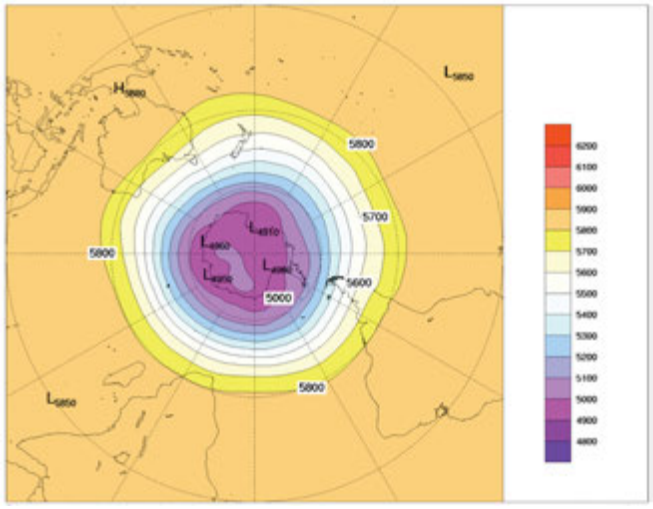

Fig. 15. Southern hemisphere spring 2012 500 hPa mean geopotential height anomalies (gpm), from a 1979–2000 climatology.

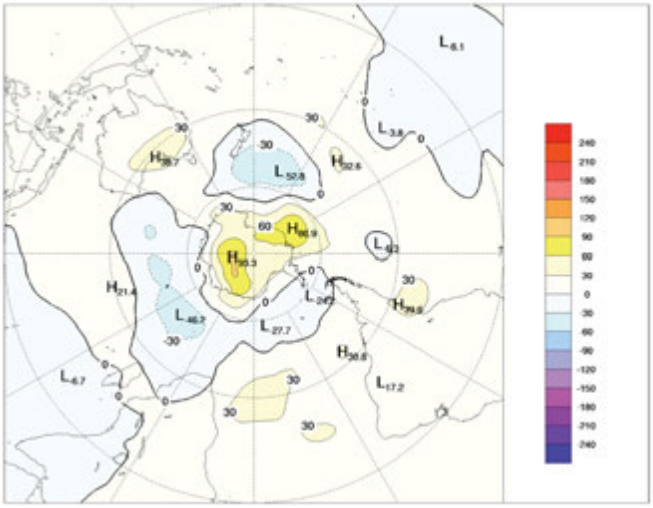

through the Tasman Sea. Further south, the positioning of the negative anomaly to the southeast of New Zealand and positive anomaly of the Amundsen Sea would have stalled transient cyclonic activity in the Ross Sea, causing cyclolysis and the positive surface pressure anomaly downstream, as per Fig. 13.

### Southern Annular Mode

The Southern Annular Mode (SAM, sometimes also referred to as the Antarctic Oscillation or AAO) is a measure of the difference between the atmospheric pressure of the high and mid-latitudes of the southern hemisphere. Positive phases of SAM are characterised by increased pressure over the extratropics, decreased pressure over Antarctica and a poleward movement of the mid-latitude band of westerly winds and associated storm tracks. Conversely, negative phases of SAM indicate decreased pressure over the extratropics, increased pressure over Antarctica, and an equatorward movement of mid-latitude westerlies. The NOAA Climate Prediction Centre routinely monitors the SAM, producing a standardised monthly SAM index[11]. During spring 2012 the SAM index switched from a positive to a negative phase (Fig. 16). This had implications on the sea ice in particular, as the positive phase, where there are strengthening westerly winds, occurred in the sea ice advance period. During spring's negative phase of SAM

[11]For more information on the SAM index from the Climate Prediction Center (NOAA), see www.cpc.ncep.noaa.gov/products/precip/CWlink/daily_ao_index/aao/aao.shtml.

(October and November), sea ice was retreating and was impacted on by a more meridional atmospheric flow causing the sea ice to retreat below the long term average by the end of November, as mentioned above.

Fig. 16. Southern Annular Mode (SAM), from January 2009 through November 2012, together with a five-month binomially weighted moving average. The departures are standardised using the 1979–2000 base period.

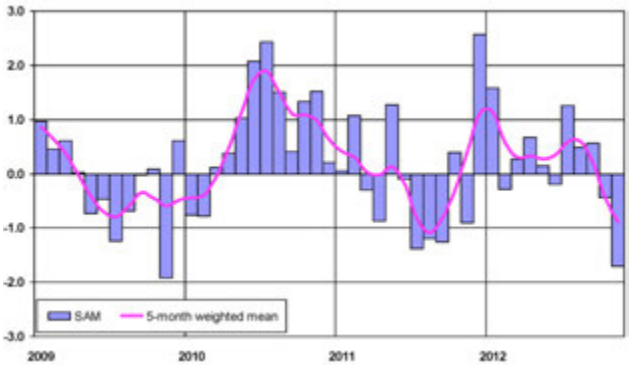


## Winds

Low-level (850 hPa) and upper-level (200 hPa) wind anomalies (from the 22-year NCEP II climatology) are shown in Figs 17 and 18 respectively. As expected from the switch in the phase of SAM, the 850 hPa anomalies are not large anywhere, although the patterns of relatively weak anomalies are consistent with the MLSP anomalies above. In particular the cyclonic anomalies to the southeast of New Zealand coincide with low pressure systems in that region. Across the equatorial Pacific there is little consistency in the anomalous flow, suggesting neither a strengthening nor weakening of the Walker Circulation—consistent with the neutral ENSO conditions discussed above. Over Australia the anomalous flow is generally northeast to northerly, except over Western Australia where there would have been a tendency for more convergence of easterly and westerly systems. Atmospheric flow through the Tasman Sea is generally from the southwest, consistent with the steering pattern showed in the 500 hPa geopotential height anomalies from Fig. 15.

The upper 200 hPa wind anomalies show a strengthening of the southern subtropical jet at various places, including to

Fig. 17. Global spring 2012 850 hPa vector wind anomalies (m $s^{-1}$). The anomaly field is not shown over areas of elevated topography.

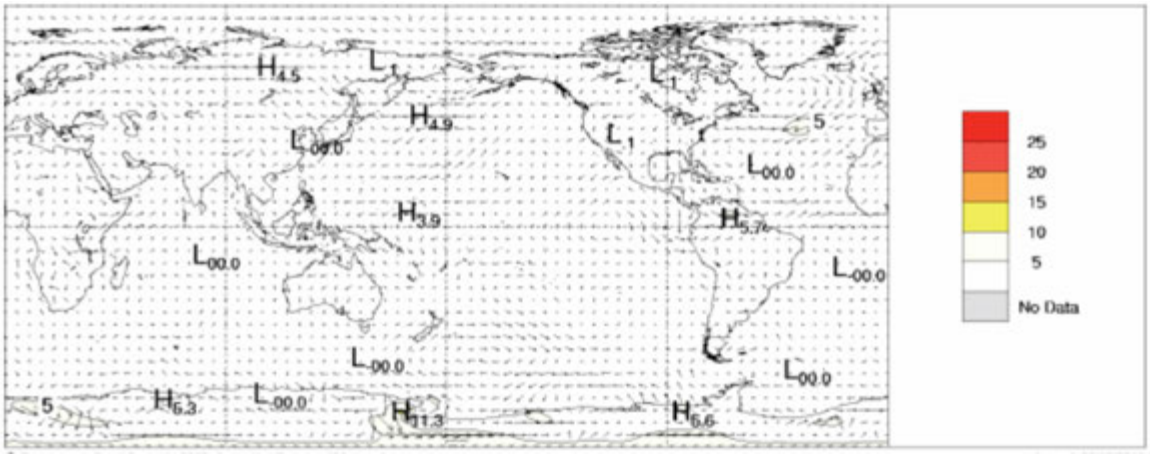


Fig. 18. Global spring 2012 200 hPa vector wind anomalies (m $s^{-1}$).

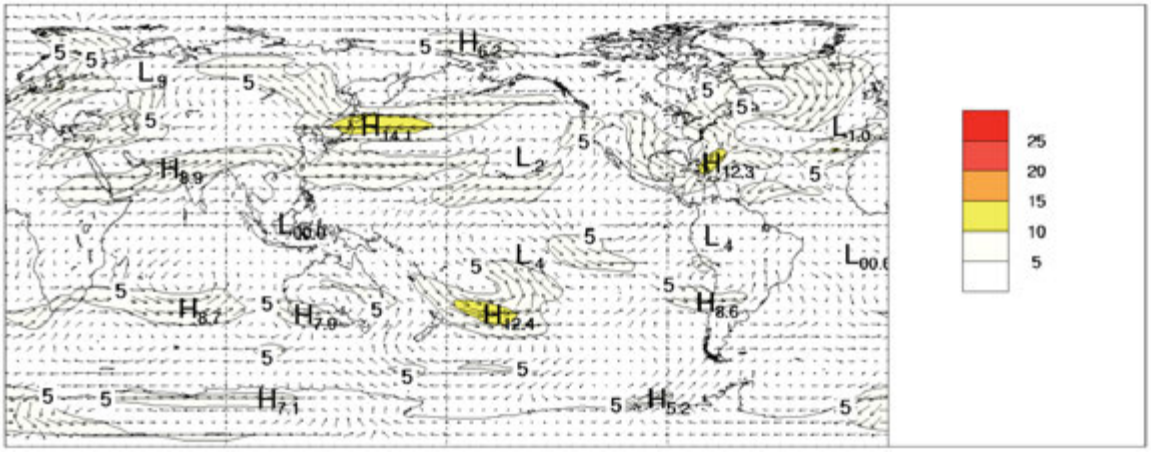

the east of New Zealand which would be responsible for the enhanced convection, increased rainfall and cyclonic activity to the right exit of this anomalous jet. This jet also runs along the line of the SPCZ and is coincident with a band of reduced OLR.

## Australian region

### Rainfall

Figures 19 and 20 show the Australian spring 2012 rainfall totals and rainfall deciles. Rainfall deciles reflect the phase of the IOD. A positive IOD SST pattern has been shown to be associated with drier than normal conditions over central and southern Australia. However, parts of Western Australia had their wettest spring on record. Western Australia's rainfall is the result of a convergent atmospheric pattern, as shown in the 850 hPa wind anomalies; relatively moist north to northwesterly winds coming in off the Indian Ocean converging with relatively dry air mass coming across the continent from the east. Several rainfall events contributed to the wetter than normal conditions over Western Australia.

Fig. 19. Australian spring 2012 rainfall totals (mm) for Australia.

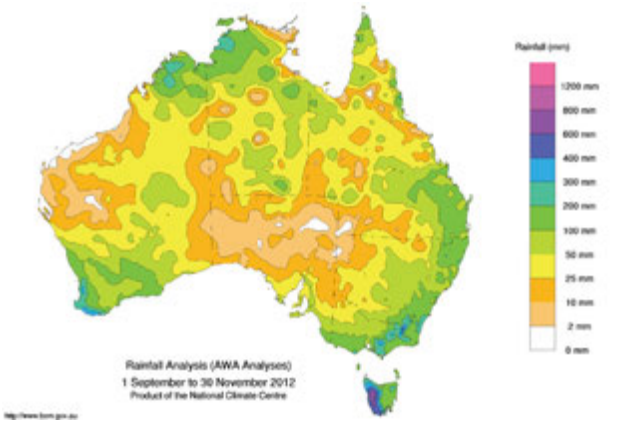


Fig. 20. Australian spring 2012 rainfall deciles for Australia: decile ranges based on grid-point values over the springs for 1900–2012.

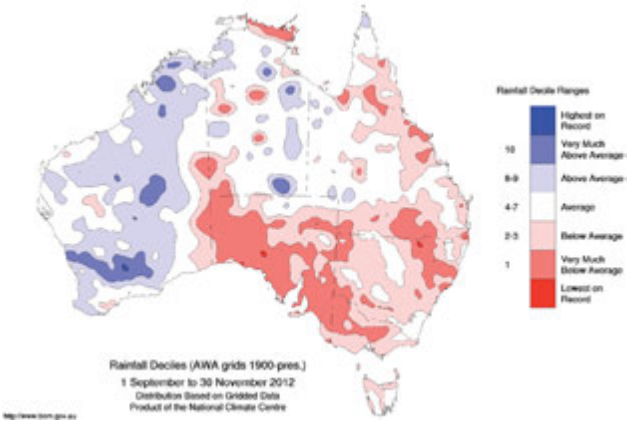


Early in September a strong cold front moved across western parts of Western Australia bringing 24 hour rainfall totals of 40 to 70 mm in some areas. Further good falls of rain fell around 24 and 25 October and again in late November. Warmun observed 102.0 mm in the 24 hours to 9.00 am on the 29th, which is its wettest November and spring day in 82 years of record. Overall Western Australia received 21 per cent above average rainfall for spring (Table 1) and was the only State to record above average rainfall for this season.

On average Australia received well below average rainfall (–27 per cent) for the season and ranked as its 33rd driest spring from 113 years of record (Table 1). This deficit was largely influenced by the three large States of Queensland (–42 per cent), New South Wales (–45 per cent) and South Australia (–69 per cent). South Australia recorded its 3rd lowest spring rainfall, with an average of 16.0 mm across the State (the record is 11.4 mm in 1963). These State rainfall figures are quite different from those of the previous (2011) spring which saw every State except Tasmania and Victoria record well above average rainfall. The return to relatively drier conditions in Queensland is a reflection of the neutral ENSO conditions and standard climate variability.

The seasonal rainfall figures mask considerable variability in the rainfall across the continent over this time. During September some stations in the Northern Territory recorded their highest September rainfall on record, while rainfall was well below average across central Western Australia, South Australia, New South Wales and Victoria. In October only the northwestern coast of Western Australia, coastal southern New South Wales and Queensland's Peninsula region had above average rainfall. Australia's wettest day for spring 2012 was 233.0 mm recorded at Ulladulla in New South Wales on 12 October. This was closely followed by 229.0 mm recorded at Cooran in Queensland on 18 October. The November 2012 rainfall decile pattern is more indicative of the total spring 2012 rainfall decile pattern, except that parts of the Northern Territory received well above average rainfall.

A summary of the rainfall ranks and extremes are shown in Table 1 for each State and Territory, with corresponding rainfall deciles (e.g. highest and lowest on record) provided in Table 2.

### Drought

Overall, compared to the rainfall deficiencies in winter 2012, drought conditions averaged over the entire continent eased somewhat during spring 2012, with predominantly Western Australia's rainfall contributing to this (Table 1). However Queensland, New South Wales, Victoria and South Australia saw expansions in their areas of severe deficiency in rainfall from those of winter 2012. In particular, more than half of South Australia recorded decile 1 rainfall during spring 2012, with a severe deficiency of over one third of the State.

Table 1. Summary of the seasonal rainfall ranks and extremes on a national and State basis for spring 2012. The ranking in the 2nd last column goes from 1 (lowest) to 113 (highest) and is calculated over the years 1900–2012.

| *Region* | *Highest seasonal total (mm)* | *Lowest seasonal total (mm)* | *Highest daily total (mm)* | *Area-averaged rainfall (mm)* | *Rank of area-averaged rainfall* | *% difference from mean* |
|---|---|---|---|---|---|---|
| Australia | 970.4 at Mount Read (Tas.) | 0.0 at several locations | 233.0 at Ulladulla (NSW), 12 October | 53 | 33 | -27 |
| Queensland | 560.0 at Bellenden Ker Top | 0.0 at Abingdon Downs Station | 229.0 at Cooran TM, 18 October | 49 | 25 | -42 |
| New South Wales | 517.2 at Perisher Valley | 0.0 at Broken Hill (Waterbag) | 233.0 at Ulladulla, 12 October | 68 | 17 | -45 |
| Victoria | 492.4 at Mount Baw Baw | 13.0 at Murray Lock Number 9 | 94.4 at Burrowye Station, 8 November | 110 | 11 | -39 |
| Tasmania | 970.4 at Mount Read | 93.0 at Hobart Airport | 52.4 at Liffey, 6 September | 314 | 36 | -14 |
| South Australia | 133.8 at Kuitpo Forest Reserve | 1.2 at Leigh Creek (Pfitzners Well) and Moomba Airport | 32.0 at Todmorden, 7 November | 16 | 3 | -69 |
| Western Australia | 417.3 at Walpole | 0.0 at several stations | 102.0 at Warmun, 29 November | 50 | 87 | +21 |
| Northern Territory | 329.5 at Channel Point | 0.0 at several stations | 115.5 at Roper River Mataranka, 30 November | 59 | 58 | -13 |

Table 2. Percentage areas in different categories for spring 2012 rainfall. 'Severe deficiency' denotes rainfall at or below the 5th percentile. Areas in 'decile 1' include those in 'severe deficiency' which in turn include those which are 'lowest on record'. Areas in 'decile 10' include those which are 'highest on record Percentage areas of highest and lowest on record are given to two decimal places because of the small quantities involved; other percentage areas to one decimal place.

| *Region* | *Lowest on record* | *Severe deficiency* | *Decile 1* | *Decile 10* | *Highest on record* | *% difference from mean* |
|---|---|---|---|---|---|---|
| Australia | 0.22 | 7.5 | 15.8 | 3.6 | 0.06 | –27 |
| Queensland | 0.09 | 3.9 | 11.5 | 0.0 | 0.00 | –42 |
| New South Wales | 0.74 | 7.7 | 24.0 | 0.0 | 0.00 | –45 |
| Victoria | 0.00 | 13.4 | 42.1 | 0.0 | 0.00 | –39 |
| Tasmania | 0.00 | 0.0 | 0.9 | 0.0 | 0.00 | –14 |
| South Australia | 0.67 | 35.1 | 58.9 | 0.0 | 0.00 | –69 |
| Western Australia | 0.00 | 0.5 | 1.6 | 9.6 | 0.19 | +21 |
| Northern Territory | 0.17 | 3.7 | 7.3 | 2.6 | 0.00 | –13 |

### Temperature

Figures 21 and 22 show spring 2012 maximum temperature anomalies and maximum temperature deciles (relative to a reference period of 1961–1990) respectively. Spring maximum temperatures across Australia were mostly warmer than normal. Averaged across the nation, maximum temperatures were 1.73 °C above normal and it was the third-warmest spring in 103 years (Table 3). Western Australia recorded its second warmest spring average maximum temperatures on record and South Australia its equal second warmest, with anomalies of +1.66 °C and +2.74 °C respectively. All States except Tasmania ranked in their respective top ten warmest springs, with the Northern Territory equal fourth, Queensland sixth and New South Wales and Victoria seventh. Tasmania's maximum temperature was the 11th warmest on record.

Most of the country was more than 1 °C warmer than usual, with temperatures further north generally closer to normal. A broad area of the southern inland experienced temperatures more than 2 °C above normal, with isolated pockets more than 3 °C above normal over the South Australian–Queensland border and just north of the Great Australian Bight.

Figures 23 and 24 show the spring 2012 minimum temperature anomalies and minimum temperature deciles (relative to a reference period of 1961–1990) respectively. Minimum temperatures during spring were generally warmer than normal over large parts of western and southern Australia, with temperatures generally closer to normal across the remainder of the country. For Australia as a whole, minimum temperatures were 0.44 °C above normal, ranking as 19th out of 103 years. The only State to fall in the top ten of their respective records was Western Australia, recording its third-warmest minimum temperatures on record (with an anomaly of +0.92 °C). Despite experiencing a close to normal month, Queensland had its coolest average spring minimum temperatures since 1994 (18 years).

Fig. 21. Australian spring 2012 maximum temperature anomalies (°C).

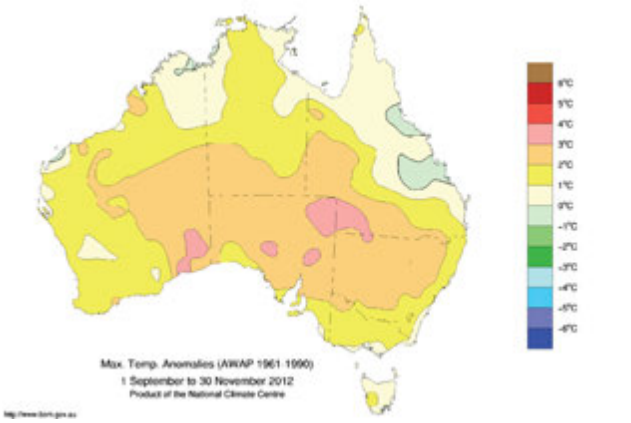


Fig. 22. Australian spring 2012 maximum temperature deciles: decile ranges based on grid-point values over the springs for 1911–2012.

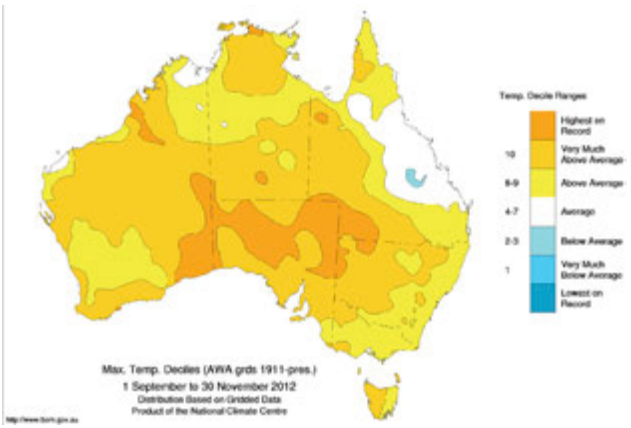


Fig. 23. Australian spring 2012 minimum temperature anomalies (°C).

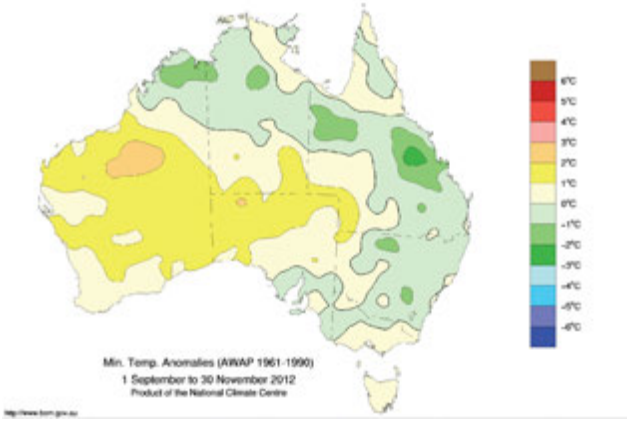


Fig. 24. Australian spring 2012 minimum temperature deciles: decile ranges based on grid-point values over the springs for 1911–2012.

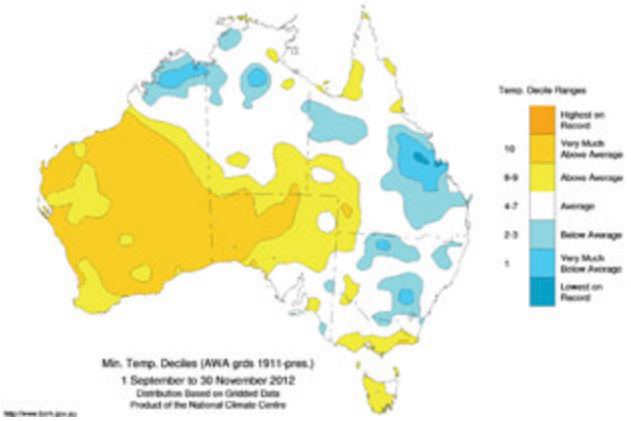


Minimum temperatures more than 1 °C above normal were measured across the Pilbara, Gascoyne, and Interior Districts of Western Australia, and extended from southeast Western Australia to the South Australia–Queensland border. Isolated pockets more than 1 °C below normal were measured across parts of the northern tropics and eastern Australia, with the majority of the country within 1 °C of normal.

Towards the end of November, exceptional heat was experienced across central and southeastern Australia. During this event, many stations measured their warmest spring day on record. Notably, five sites in Victoria broke the existing State record, with Ouyen's 45.8 °C on the 29th the new Victorian highest spring temperature (previous record held by Mildura, with 44.5 °C on 17 November 1980). Minimum temperatures were also affected, with Oodnadatta breaking the highest South Australian November minimum temperature on record (with 32.3 °C on 29 November). This exceptional spring heat, together with the dry conditions discussed above, would leave this area of the continent vulnerable to summer bushfires. For more on the November 2012 heat wave see Special Climate Statement 41, Bureau of Meteorology 2012.

A summary of the maximum and minimum temperature ranks and extremes for each State and Territory are provided in Tables 3 and 4 respectively, with corresponding maximum and minimum temperature deciles given in Table 5.

## Ozone

### Antarctic Ozone Hole

Monthly mean temperatures in the lower stratosphere above Antarctica during 2012 were generally close to or slightly below the 1979–2011 climatological average from January to July, but showed marked warming from mid-spring to early summer, particularly at and below the 50 hPa level (WMO, 2012). The warming of the Antarctic lower stratosphere occurred while both the stratospheric (50 hPa) Quasi-Biennial Oscillation (QBO) and stratospheric (20 hPa) SAM indices were in a strongly negative state (refer Fig. 16 for the phase of the tropospheric SAM) which would tend to favour a weak and disturbed stratospheric polar vortex

Table 3. Summary of the seasonal maximum temperature ranks and extremes on a national and State basis for spring 2012. The ranking in the last column goes from 1 (lowest) to 103 (highest) and is calculated over the years 1950–2012*.

| *Region* | *Highest seasonal mean maximum (°C)* | *Lowest seasonal mean maximum (°C)* | *Highest daily temperature (°C)* | *Lowest daily maximum temperature (°C)* | *Area-averaged temperature anomaly (°C)* | *Rank of area-averaged temperature anomaly* |
|---|---|---|---|---|---|---|
| Australia | 39.7 at Fitzroy Crossing (WA) | 7.7 at Mount Hotham (Vic.) | 46.4 at Roebourne (WA), 15 November | –4.5 at Thredbo (Top Station) (NSW), 29 September | +1.73 | 101 |
| Queensland | 37.6 at Century Mine | 23.5 at Applethorpe | 44.7 at Century Mine, 21 November | 11.0 at Stanthorpe, 12 October | +1.29 | 97 |
| New South Wales | 31.4 at Mungindi | 8.5 at Thredbo (Top Station) | 46.2 at Poonca-rie, 29 November | –4.5 at Thredbo (Top Station), 29 September | +2.28 | 96 |
| Victoria | 26.5 at Mildura | 7.7 at Mount Hotham | 45.8 at Ouyen, 29 November | –4.2 at Mount Hotham, 29 September | +1.58 | 96 |
| Tasmania | 18.8 at Bushy Park | 8.4 at Mount Wellington | 34.2 at Orford, 30 November | –1.8 at Mount Wellington, 29 September | +0.83 | 92 |
| South Australia | 33.2 at Moomba | 17.9 at Mount Lofty and Parawa | 46.0 at Marree Comparison, 29 November | 7.8 at Mount Lofty, 11 October | +2.74 | 102.5 |
| Western Australia | 39.7 at Fitzroy Crossing | 19.7 at Cape Leeuwin, North Walpole and Windy Harbour | 46.4 at Roebourne, 15 November | 9.8 at Mount Barker, 4 September | +1.66 | 102 |
| Northern Territory | 38.4 at Timber Creek | 30.4 at McCluer Island | 44.1 at Yulara, 25 November | 16.5 at Arltunga, 29 September | +1.43 | 100.5 |

*A high-quality subset of the temperature network is used to calculate the spatial averages and rankings shown in Table 4 (maximum temperature) and Table 5 (minimum temperature). These averages are available from 1950 to the present. As the anomaly averages in the tables are only retained to two decimal places, tied rankings are possible.

Table 4. Summary of the seasonal minimum temperature ranks and extremes on a national and State basis for spring 2012. The ranking in the last column goes from 1 (lowest) to 103 (highest) and is calculated over the years 1950–2012.

| *Region* | *Highest seasonal mean minimum (°C)* | *Lowest seasonal mean minimum (°C)* | *Highest daily minimum temperature (°C)* | *Lowest daily temperature (°C)* | *Area-averaged temperature anomaly (°C)* | *Rank of area-averaged temperature anomaly* |
|---|---|---|---|---|---|---|
| Australia | 26.1 at McCluer Island (NT) | 0.4 at Thredbo (Top Station) (NSW) | 32.3 at Oodnadatta (SA), 29 November | –9.0 at Cooma Airport (NSW), 2 September | +0.44 | 85 |
| Queensland | 24.8 at Coconut Island | 8.0 at Applethorpe | 30.5 at Ballera, 27 November | –4.0 at Stanthorpe, 2 September | –0.04 | 57 |
| New South Wales | 16.4 at Byron Bay | 0.4 at Thredbo (Top Station) | 30.9 at Wanaaring, 30 November | –9.0 at Cooma Airport, 2 September | +0.10 | 59 |
| Victoria | 11.7 at Gabo Island | 0.7 at Mount Hotham | 26.3 at Yarrawonga, 30 November | –7.2 at Mount Hotham, 2 September | +0.29 | 80.5 |
| Tasmania | 10.4 at Swan Island | 0.9 at Mount Wellington | 19.3 at Strahan, 30 November | –7.0 at Liawenee, 1 September | +0.13 | 76 |
| South Australia | 16.5 at Oodnadatta | 5.9 at Keith (Munkora) | 32.3 at Oodnadatta, 29 November | –1.9 at Murray Bridge (Pallama-na Aerodrome), 25 September | +0.89 | 91.5 |
| Western Australia | 24.2 at Wyndham | 6.9 at Wandering | 31.4 at Wittenoom, 15 November | –2.5 at Eyre, 30 September | +0.92 | 101 |
| Northern Territory | 26.1 at McCluer Island | 14.1 at Arltunga | 29.6 at Ngukurr, 18 November | –0.4 at Arltunga, 10 September | +0.07 | 65 |

Table 5. Percentage areas in different categories for spring 2012. Areas in 'decile 1' include those which are 'lowest on record'. Areas in 'decile 10' include those which are 'highest on record'. Percentage areas of highest and lowest on record are given to two decimal places because of the small quantities involved; other percentage areas to one decimal place. Grid-point deciles calculated with respect to 1911–2012.

| *Region* | *Maximum temperature* | | | | *Minimum temperature* | | | |
|---|---|---|---|---|---|---|---|---|
| | *Lowest on record* | *Decile 1* | *Decile 10* | *Highest on record* | *Lowest on record* | *Decile 1* | *Decile 10* | *Highest on record* |
| Australia | 0.00 | 0.0 | 64.8 | 11.62 | 0.21 | 3.6 | 27.5 | 0.00 |
| Queensland | 0.00 | 0.0 | 40.8 | 6.75 | 0.91 | 8.9 | 1.0 | 0.00 |
| New South Wales | 0.00 | 0.0 | 62.4 | 6.95 | 0.00 | 3.6 | 0.0 | 0.00 |
| Victoria | 0.00 | 0.0 | 25.6 | 0.00 | 0.00 | 0.0 | 1.6 | 0.00 |
| Tasmania | 0.00 | 0.0 | 64.9 | 0.00 | 0.00 | 0.0 | 0.0 | 0.00 |
| South Australia | 0.00 | 0.0 | 98.0 | 46.99 | 0.00 | 0.0 | 38.6 | 0.00 |
| Western Australia | 0.00 | 0.0 | 72.0 | 8.72 | 0.00 | 2.4 | 67.3 | 0.00 |
| Northern Territory | 0.00 | 0.0 | 66.1 | 2.41 | 0.00 | 2.4 | 1.5 | 0.00 |

Fig. 25. Antarctic Ozone Hole area, defined as the region where total column ozone is less than 220 Dobson Units, for 2012 (thick black line) based on measurements from the Dutch-Finnish OMI instrument carried by NASA's Aura satellite, as compiled by CSIRO, compared to previous years.

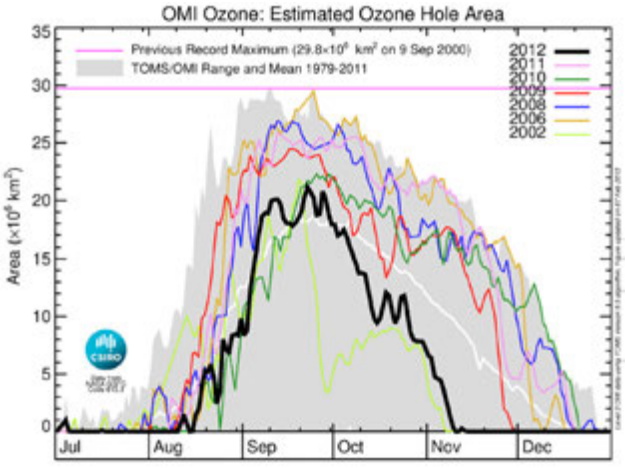


Fig. 26. Mean spring (September–October–November) total ozone measured by Dobson spectrophotometer 1990–2012 at Darwin (top), Brisbane (middle) and Melbourne (bottom). The dotted line denotes the 1990–2012 average.

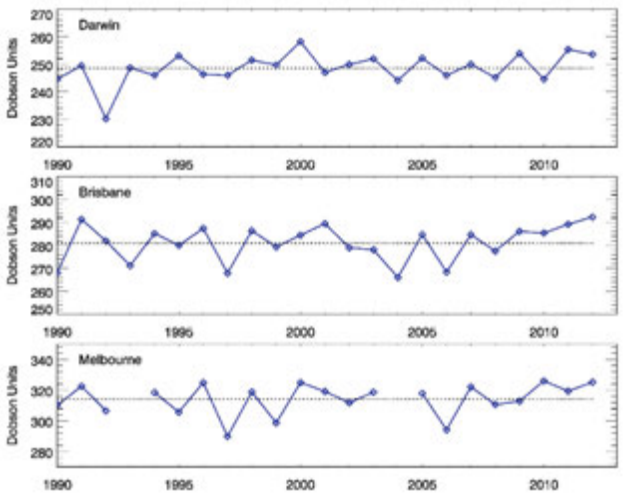


(Baldwin and Dunkerton 1998, 2001). Indeed, episodes of strong southward heat transport occurred from early July, and culminated with the rapid decrease in the area of the polar vortex from mid-October (WMO 2012), and corresponding rapid decline in the area of the Ozone Hole (Fig. 25). Of note was the complete breakdown of the vortex in early December, causing one of the earliest disappearance dates for the ozone hole (around 15 November) since 1988 (excluding 2002, when the vortex was anomalously disturbed and small).

The maximum daily ozone hole area for 2012 was 21.2 million km$^2$, ranking as only the 23rd largest measured and the smallest since 1988.

### Australia

Figure 26 shows spring mean total ozone for the years 1990 to 2012, as measured at three Bureau Dobson spectrophotometer observing sites of Darwin, Brisbane and Melbourne. Although day-to-day variability is high at this time of year, during which the maximum in the annual cycle occurs, when averaged over a season the main influences are the phase of the stratospheric QBO and of the 11-year solar cycle. Over a decadal scale the influence of stratospheric halogen loading, which increased until the mid 1990s and has since decreased, is also clear. The anomalously low 1992 Darwin value is associated with the eruption of Mt Pinatubo in June 1991.

In spring 2012 the solar cycle was at mid-levels and the QBO was in a negative (westward) phase, associated with higher values of ozone in the sub-tropics and mid-latitudes. At all three sites the spring mean ozone in 2012 was at the higher side of the 1990–2011 range—Darwin 254 DU (4th highest), Brisbane 292 DU (the highest) and Melbourne 325 DU (the 2nd highest). The highest single ozone daily average was 398 DU on 29 September measured in Melbourne.

## Acknowledgments

The author wishes to thank Dr Melanie Webb and Lorien Martin for their assistance in providing comments and advice on earlier drafts of this paper.

## References

Baldwin, M. P. and Dunkerton, T.J. 1998. Quasi-biennial modulations of the Southern Hemisphere stratospheric polar vortex, *Geophys. Res. Lett., 25,* 3343–46.

Baldwin, M.P. and Dunkerton, T.J. 2001. Stratospheric harbingers of anomalous weather regimes. *Science, 294,* 581–4.

Bureau of Meteorology. 2012a. Record-breaking La Niña events: An analysis of the La Niña life cycle and the impacts and significance of the 2010–11 and 2011–12 La Niña events in Australia. Available from http://www.bom.gov.au/climate/enso/history/ln-2010-12/index.shtml ISBN: 978 0 642 70621 8.

Bureau of Meteorology. 2012b. Extreme November heat in eastern Australia. *Special Climate Statement 41*, Bureau of Meteorology, Australia. Accessible via http://www.bom.gov.au/climate/current/special-statements.shtml

Cottrill, D.A. 2012. Seasonal climate summary southern hemisphere (spring 2011): La Niña returns. *Aust. Met. Oceanogr. J., 62,* 179–92.

Donald, A., Meinke, H., Power, B., Maia, A.H.N., Wheeler, M.C., White, N., Stone, R.C. and Ribbe. J. 2006. Near-global impact of the Madden-Julian Oscillation on rainfall. *Geophys. Res. Lett., 33*, L09704.

Ganter, C. 2010. Seasonal climate summary southern hemisphere (winter 2010): A fast developing La Niña. *Aust. Met. Oceanogr. J., 61,* 125–35.

Holland, P.R. and Kwok, R. 2012 Wind-driven trends in Antarctic sea-ice drift. *Nature Geoscience, 5,* 872–5.

Lovitt, C. 2011. Seasonal climate summary southern hemisphere (spring 2010): La Niña strengthens. *Aust. Met. Oceanogr. J., 61,* 185–95.

Kanamitsu, M., Ebisuzaki, W., Woollen, J., Yang, S.-K, Hnilo, J.J., Fiorino, M. and Potter, G.L. 2002. NCEP-DOE AMIP-II Reanalysis (R-2). *Bull. Am. Meteorol. Soc., 83,* 1631–43.

Kuleshov, Y. Qi, L., Fawcett, R. and Jones, D. 2009. 'Improving preparedness to natural hazards: Tropical cyclone prediction for the Southern Hemisphere,' in: Gan, J. (Ed.), *Advances in Geosciences, Vol. 12 Ocean Science*, World Scientific Publishing, Singapore, 127–43.

Martin, L. 2013. Seasonal climate summary southern hemisphere (autumn 2012): the transition from La Niña to neutral. *Aust. Met. Oceanogr. J., 63,* 249–59.

Massom, R., Reid, P., Stammerjohn, S., Raymond, B., Fraser, A. and Ushio, S. 2013. Change and Variability in East Antarctic Sea Ice Seasonality, 1979/80–2009/10, *PLoSONE, 8,* e64756.

McGregor, S.A., Timmermann, A., Schneider, N., Stuecker, M.F. and England, M.H. 2012. The effect of the South Pacific Convergence Zone on the termination of El Niño events and the meridional asymmetry of ENSO, *J. Clim., 25,* 5566–86.

Pepler, A. 2013. Seasonal climate summary southern hemisphere (winter 2012): Dry conditions return to Australia. *Aust. Met. Oceanogr. J.,* in press.

Reynolds, R.W., Rayner, N.A., Smith, T.M., Stokes, D.C. and Wang, W. 2002. An improved in situ and satellite SST analysis for climate. *J. Clim., 15,* 1609–25.

Risbey, J.S., Pook, M.J., McIntosh, P.C., Wheeler, M.C. and Hendon, H.H. 2009. On the remote drivers of rainfall variability in Australia. *Mon. Wea. Rev., 137,* 3233–53.

Stammerjohn, S.E., Martinson, D.G., Smith, R.C., Yuan, X. and Rind, D. 2008. Trends in Antarctic annual sea ice retreat and advance and their relation to El Nino–Southern Oscillation and Southern Annular Mode variability, *J. Geophys. Res., 113,* C03S90, doi:10.1029/2007JC004269.

Stammerjohn, S., Massom, R., Rind, D. and Martinson, D. Regions of rapid sea ice change: An inter-hemispheric seasonal comparison, *Geophys. Res. Lett., 39,* L06501.

Troup, A.J. 1965. The Southern Oscillation. *Q. J. R. Meteorol. Soc., 91,* 490–506.

Webb, M. 2012. Seasonal climate summary southern hemisphere (summer 2011–12): a mature La Niña, strongly positive SAM and active MJO. *Aust. Met. Oceanogr. J., 62,* 335–49.

Wolter, K. and Timlin, M.S. 1993. Monitoring ENSO in COADS with a seasonally adjusted principal component index. Proc. Of the 17th Climate Diagnostics Workshop, Norman, OK, NOAA/NMC/CAC, NSSL, Oklahoma Clim. Survey, CIMMS and the School of Meteorology, Univ. of Oklahoma, 52–7.

Wolter, K. and Timlin, M.S. 1998. Measuring the strength of ENSO – how does 1997/98 rank? *Weather, 53,* 315–24.

World Meteorological Organisation (WMO) Antarctic Ozone Bulletin No. 6/2012 (URL http://www.wmo.int/pages/prog/arep/documents/ant-bulletin-6-2012.pdf)

Zhang, C. 2005. Madden–Julian Oscillation. *Rev. Geophys. 43,* RG2003, 36pp, doi:10.1029/2004RG000158.